J Mater Sci (2011) 46:1110–1123
DOI 10.1007/s10853-010-4880-y

Effect of aspect ratio on large deformation and necking of polyethylene

S. Muhammad · P.-Y. B. Jar

Received: 29 April 2010 / Accepted: 28 August 2010 / Published online: 14 September 2010

Abstract Objective of the study is to examine influence of aspect ratio of rectangular cross-section on the tri-axial stress state developed by necking in tensile specimens of polyethylene. The first part of the paper presents an experimental study that used two types of high-density polyethylene (HDPE) as sample material to identify the thickness-dependent relationship between engineering stress and elongation from tensile tests. The experimental study also shows that thinner specimens, i.e. higher aspect ratio, have lower neck propagation speed and higher flow stress, thus higher rate of energy consumption for the neck propagation. The second part of the paper presents finite element simulation of large deformation and necking in HDPE when subjected to uni-axial tension. True stress–strain relationship and governing equation for visco-plastic deformation are determined from the finite element simulation based on experimental data for the two HDPEs, which reveals influence of aspect ratio of cross-section on the stress state during the necking process. Results from the study indicate that plane-stress condition prevails when the aspect ratio increases, i.e. by decreasing the specimen thickness. The finite element simulation also supports the observation that necking in specimens with higher aspect ratio, i.e. thinner specimens, generates higher percentage of reduction in the thickness direction but lower in the width direction. The overall capability for the deformation endurance was found to improve by reducing the specimen thickness. The paper concludes that finite element simulation has successfully demonstrated the influence of aspect ratio of the cross-section on the stress state in the necking process. The paper also concludes that by combining experimental testing and finite element simulation, time-dependent deformation behaviour can be separated from the time-independent deformation behaviour, which is almost impossible to achieve based on the experimental techniques that rely purely on measurement only.

S. Muhammad (✉) · P.-Y. B. Jar
Department of Mechanical Engineering, University of Alberta, Edmonton, AB T6G 2G8, Canada
e-mail: souvenir@ualberta.ca

Introduction and background

Large deformation, especially when necking occurs, has attracted attention from many research groups around the world [1–8]. This is not only because understanding this behaviour has great potential to advance knowledge on material deformation, but also due to the common occurrence of necking in the fracture process of materials with high toughness. Previous studies have shown that numerical simulation, when combined with experimental measurement, is a promising tool to determine material properties in large deformation. Among materials of interest in those studies, high-density polyethylene (HDPE) exhibits strong strain-hardening behaviour in large deformation, thus generating very stable neck development. The capability of stable necking before fracture is an important factor for HDPE in load-bearing applications, such as pipeline and pressure vessels that are used in the distribution network for oil and gas. In addition, large straining is required in production of high-strength polymer fibers [9], for which the knowledge on necking facilitates the control of the production process. However, in spite of the importance of polymer necking in many industrial applications and extensive studies on its occurrence [1–19], mechanisms involved and criteria required are yet to be fully quantified. For polyethylene, the challenge is aggravated by the involvement of time-dependent deformation

behaviour. At the time when this manuscript is prepared, only several studies [2, 6] are able to consider the time-dependent deformation behaviour in computer simulation to mimic the necking process accurately.

Most of the previous works on the necking behaviour [2–4, 6, 9, 10] were focused on the effects of parameters such as strain rate, temperature and initial imperfection size on the neck development. Little attention has been paid to the influence of aspect ratio of the cross-section. Thus, objective of the current study is to gain fundamental understanding of the influence of aspect ratio on the neck development, and to reveal the associated variation of stress state in the necking zone. In this work, aspect ratio is varied through thickness change for standard dog-bone specimens that are commonly used for simple tensile test.

The paper consists of two parts: (i) experimental investigation to capture variation of the deformation behaviour and mechanical properties during the necking process, and (ii) computer simulation based on finite element (FE) method to determine the constitutive equation that can accurately mimic the experimental observations. Results from the study are used to enlighten stress state generated during the necking process. In the remaining part of this section, two brief reviews of previous work on large deformation and necking of polymers are presented, one on experimental measurement and the other on FE simulation.

Experimental measurement

G'Sell and Jonas [12] and Kwon and Jar [18] gave detailed description on the neck development in simple tensile test. The former presents experimental curves of load versus elongation and engineering stress versus strain for polyvinyl chloride and HDPE, in which initiation and stabilisation points on the curves for neck development are identified. The latter quantifies change of cross-section and nominal stress in HDPE during the neck development. Kwon and Jar suggest that neck development in HDPE occurs in two stages, for neck inception and neck propagation, respectively. In addition, following Hill's [20] approach they modified the neck initiation criterion determined from the simple tensile test, and applied it to the neck development in double-edge-notched tensile test. In an experimental study, G'Sell et al. [9] evaluated stress triaxiality (as defined in Ref. [21]) in cylindrical tensile specimens, and suggested that the section with a convex external profile should have very different stress triaxiality from that with a concave external profile. Later, Kwon and Jar [5] used dog-bone specimens of rectangular cross-section to demonstrate the non-uniform stress state on the cross-section at the neck inception stage. Other studies on various polymers [10, 19] reported true stress–strain relationship for large deformation using experimental techniques, and measured variation of volume strain during the neck development.

Finite element simulation

Finite element method has been widely used in literature to simulate large deformation and necking of polymers like HDPE [e.g., 1–8]. However, most studies paid little attention to the establishment of proper constitutive equation to generate the deformation. Among the few attempts that paid attention to this, such as the work by Neale and Tugcu [1], Fager and Bassni [7] and Masud [8], the constitutive equation was rarely validated by experimental data.

To our knowledge, only four papers in the literature used experimental data to evaluate results from FE simulation. Boyce and Arruda [2], by considering rotation and alignment of molecular chain segments, developed a constitutive model to simulate necking in glassy polymers that exhibit both strain softening and straining hardening. Although they compared the simulation results with experimental data, we do not think that the agreement is close enough to fully validate the model, especially when subjected to tensile loading. As a result, the model was not adopted here to investigate the effects of aspect ratio on the neck development. It should be noted that Wu and Van Der Giessen [3] used a constitutive model similar to the model developed by Boyce and Arruda, to study the necking phenomenon in glassy polymers. Variables considered in that study include initial imperfection size, strain softening and hardening parameters, strain rate, as well as specimen geometry. Although similar to the model by Boyce and Arruda, the model by Wu and Van Der Giessen uses material properties that could be determined experimentally, the simulation results were not explicitly validated using experimental data. Furthermore, aspect ratio was not included in the study as a variable for the specimen geometry.

Tomita and Hayashi [4] proposed an iterative process to identify model parameters that can accurately simulate the necking process at different temperatures and strain rates. The results were used to discuss effects of strain rate, temperature and stress triaxiality on the deformation behaviour during the necking process. Their iterative process was further modified by Kwon and Jar [5], from which the results exhibited a close agreement with the experimental observation on HDPE in both uni-axial tensile and double-edge-notched tensile tests. The constitutive model proposed by Kwon and Jar is through a combination of stress–strain relationships for different ranges of deformation, which are available in the literature and given below with the expressions (Eq. 1(a) [1, 14, 16], 1(b) [22], 1(c) [23] and 1(d) [12, 13])

$$\sigma(\varepsilon) = \begin{cases} E\varepsilon & \text{for } \varepsilon \le \varepsilon_y \quad \text{(a)} \\ d\left[\{a(\varepsilon+b)\}^{(c-1)} - \{a(\varepsilon+b)\}^{(-c)}\right] + e & \text{for } \varepsilon_y \le \varepsilon \le \varepsilon_n \quad \text{(b)} \\ \alpha k \varepsilon^N & \text{for } \varepsilon_n \le \varepsilon \le \varepsilon_t \quad \text{(c)} \\ k\exp(M\varepsilon^\beta) & \text{for } \varepsilon \ge \varepsilon_t \quad \text{(d)} \end{cases}, \tag{1}$$

in which unit for σ is MPa, ε_y represents the transitional strain between linear and nonlinear part of the elastic deformation, ε_n the strain for on-set of necking and ε_t the transitional strain for the strain-hardening part of the plastic deformation.

Li and Buckley [6] also presented a numerical study on necking of glassy polymers by employing a glass-rubber constitutive model at the molecular level, in which the nonlinear elastic-viscoplastic deformation is incorporated in the response to deviatoric stress, to take into account the time-dependent deformation behaviour that is known for many polymers. Although all of the above work establishes the constitutive equation for large deformation and necking, the approach adopted by Tomita and Hayashi [4] and by Kwon and Jar [5] is different from that by Boyce and Arruda [2] and by Li and Buckley [6]. The former uses a macroscopic (global) approach, with validation based on load-elongation curve and reduction of cross-section in the necking process; while the latter uses a microscopic approach based on motion at the molecular level.

In addition to the above studies on necking, it is worth mentioning that some papers in the literature have searched for explanations for the compressive yield stress being higher than the tensile counterpart for many polymers such as polyethylene and polycarbonate. Spitzig et al. [24] suggested that hydrostatic stress and its type (tension or compression) may have influenced the yielding process. Raghava et al. [25] reported possible changes of the yield surface under a wide range of loading conditions. Spitzig and Richmond [26] showed the change of tensile and compressive deformation behaviour for some polymers under various hydrostatic pressures. Similar studies were also conducted by Silano et al. [27]. Although those studies demonstrated variability of stress–strain curves by the change of hydrostatic pressure, the variation occurs only with a significant change of the hydrostatic pressure. In simple tensile tests conducted in the current study, the hydrostatic stress is mainly generated by axial load, of which the level should not be high enough to impose any significant effect on the yielding behaviour.

It should be noted that very few studies have been conducted to reveal the influence of cross-sectional dimensions on the necking behaviour, let alone its influence on the triaxial stress state during the necking process. Scarcity of information in this area provides motivation for the current study.

Problem description and research methodology

Although necking is a phenomenon commonly observed in simple tensile test of many ductile polymers, the standard method (ASTM D638) that uses specimens of rectangular cross-section does not consider the influence of aspect ratio (defined as the ratio of width to thickness of the cross-section) on the deformation. In addition, current practice on material evaluation that is based on simple tensile test results only considers results up to the yield point, despite the fact that many products rely on post-yield deformation to evaluate their reliability and damage tolerance. In view of the possible influence of aspect ratio of specimen cross-section on the post-yield deformation, we conducted experimental testing and FE simulation to understand the following phenomena: (i) variation of the necking behaviour with the change of aspect ratio, (ii) the corresponding change in the triaxial stress state and (iii) the involvement of viscoplastic deformation during the necking.

Methodology adopted in the study is firstly to identify constitutive stress–strain relationship that enables the FE model to mimic the deformation behaviour observed experimentally, which includes experimental load-elongation curve and the cross-section reduction during the necking process. In this work, validation of the FE model is based on the following experimental data:

(i) Curves of engineering stress versus elongation, with special attention paid to the peak stress position (stress value and the corresponding elongation), profile for the stress-drop section, and the flow stress level during the neck propagation, and
(ii) Reduction of the cross-section as a function of elongation at the location where the neck was initially generated.

The FE model that met the above criteria was then used to analyse variation of stress state by the change of aspect ratio on the cross-section.

The above approach for determining the constitutive relationship between stress and strain is different from the purely experimental measurement that was demonstrated by G'Sell et al. [19] who determined strains based on displacement at selected positions on the specimen surface. The experimental method by G'Sell et al. is applicable only if strain distribution is relatively uniform in the area between the selected positions. As the necking process

involves significantly inhomogeneous reduction of cross-section, the deformation clearly violates the above assumption. In a similar experimental approach, Fang et al. [10] used a three-dimensional non-contact technique, based on digital image correlation, to measure large deformation in polymers. Although this technique allows non-uniform strain distribution in the area of measurement, and has the potential to extract creep strain from the total strain, the measurement is limited to deformation on surface. When the strain on the surface does not represent the strain inside, such as the case for necking in polymers, the technique cannot be used to determine the internal strain values. As a result, techniques purely based on experimental measurement are insufficient to determine the constitutive equation when necking occurs. Instead, a new approach that combines experimental measurement with computer simulation is adopted in this study to determine the constitutive equation for the FE simulation.

Experimental

Two types of HDPE, named PE1 and PE2 here, were provided by NOVA Chemicals for the experimental investigation. Characteristics of the HDPEs, such as molecular weight, molecular weight distribution and density, are given in Table 1. HDPE pellets were firstly compression-moulded to rectangular plates with nominal thickness in the range from 2 to 10 mm. Melt flow was minimised during the moulding process to avoid molecular alignment, thus ensuring isotropy of the mechanical properties. The plates were then machined to dog-bone specimens of standard dimensions, as shown in Fig. 1. Width in the middle part of the gauge section, around 2 mm long, was reduced gradually by a maximum reduction of 0.1 mm, which corresponds to less than 1% reduction from the original width. Such width reduction was to ensure that the neck initiation occurred at the location where the extensometer was placed, in order to measure accurately the width and thickness changes during the neck development. In addition, a high resolution video camera was used to record the neck initiation and growth along the gauge length, in order to quantify the neck growth rate.

Since standard dog-bone specimen has width fixed at 13 mm, variation of aspect ratio was through change of specimen thickness from 2 to 10 mm, corresponding to change of aspect ratio from 6.5 (for 2-mm-thick specimens) to 1.3 (for 10-mm-thick specimens). Although only specimen thickness was used as the variable to change the aspect ratio, the trend presented in this paper should be universal and the constitutive equation determined applicable to mimicking the necking process in specimens of different width. It should be noted that in the beginning of this study, due to machining and polishing using 600-grit sand paper for the specimen preparation, there were concerns about the possible influence of the surface roughness on the deformation behaviour, and the influence may vary with the change of specimen width. Therefore, specimen width was kept constant to remove this concern. It turned out that all specimens used in this study fractured after the neck had been fully developed in the whole gauge section. As a result, surface roughness introduced by machining and polishing did not have any effect on the necking behaviour described in this paper.

The tensile tests were conducted using a universal testing machine (QUASAR 100) at a crosshead speed of 100 mm/min. The choice of a relatively high crosshead speed was to minimise the time for the neck initiation to be less than 30 s, in order to reduce the amount of time-dependent deformation so that a relative simple creep model could be used in the simulation to mimic the neck formation.

The experiments require measurement of width and thickness changes to determine strain values. To reduce scattering of width and thickness measurements during the necking, the measured data were smoothed using a commercial graphics software (KaleidaGraph version 3.5), based on a window size of 10 points for a data set of around 3000 points from each test.

Numerical simulation

The numerical simulation was carried out on two specimen thicknesses, 10 and 3 mm, using ABAQUS Standard (version 6.7-1). FE model for the former thickness has 4140 20-node brick elements and totally 19583 nodes, and for the latter 4620 20-node brick elements and 22183 nodes. As an example, Fig. 2 shows the mesh pattern for the 10-mm-thick model, with 1-, 2- and 3-axes designated the direction along length, width and thickness, respectively. Due to geometrical symmetry, the FE model is only

Table 1 Material characteristics for HDPE used in this study

Material designation	M_w (g mol^{-1})	M_n (g mol^{-1})	M_z (g mol^{-1})	Density, ρ (g cm^{-3})	M_w/M_n
PE1 (hexene copolymer)	182,000	17,000	935,000	0.945	10.6
PE2 (octene copolymer)	73,100	30,400	147,000	0.941	2.4

M_w weight-average molecular weight, M_n number-average molecular weight and M_z Z-average molecular weight

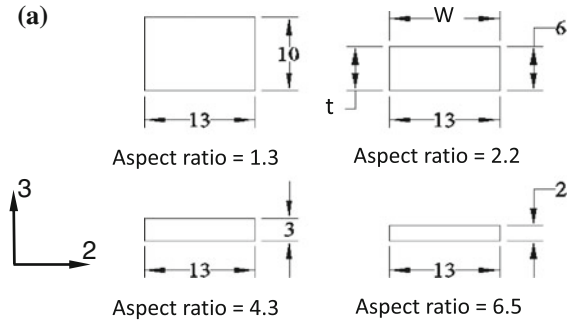

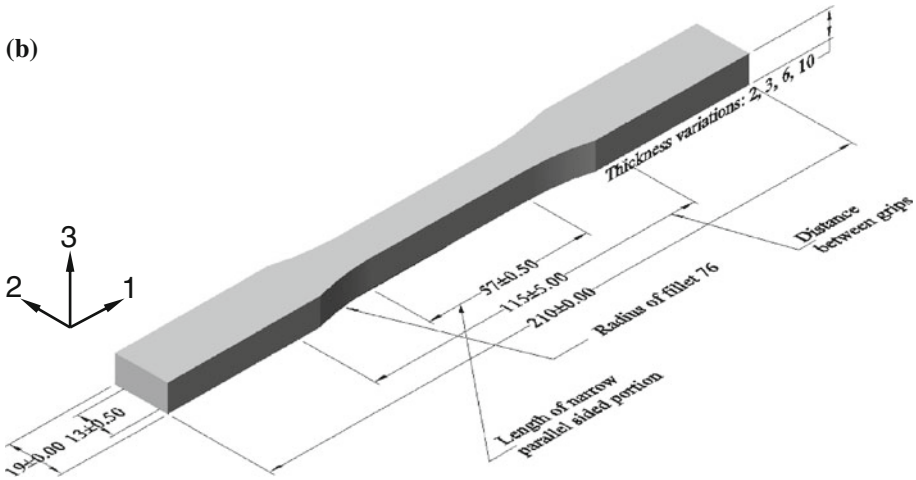

Fig. 1 **a** Cross-sectional dimensions for four different aspect ratios by change in thickness from 10 to 2 mm and **b** other dimensions of the specimen according to ASTM D638 (Type 1)

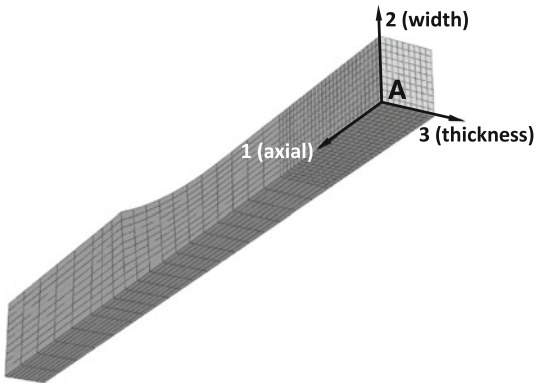

Fig. 2 Example of un-deformed FE model with origin of the co-ordinate system set at point *A*

for half of the specimen length and quarter of the cross-section. That is, point *A* in Fig. 2 is at the centre of the cross-section in the middle of the specimen. An imperfection was introduced through a tapered width reduction, to reduce the width by about 0.07% of the original value at the cross-section where point *A* is, so that necking was always initiated from there.

Plastic deformation generated in the FE model is based on J_2 flow theory, that is,

$$f(\sigma_{ij}) = \sqrt{3J_2} = \frac{1}{\sqrt{2}}\Big[(\sigma_{11}-\sigma_{22})^2+(\sigma_{22}-\sigma_{33})^2 + (\sigma_{33}-\sigma_{11})^2+ 6\left(\sigma_{12}^2+\sigma_{23}^2+\sigma_{31}^2\right)\Big]^{\frac{1}{2}} = Y \qquad (2)$$

where Y is the yield stress determined from the simple tensile test. Most of the work in the past [e.g. 1, 4, 5, 7, 14–16] assumed that the simple tensile test introduces uni-axial stress state in the gauge section, which ignores the transverse normal stresses (σ_{22} and σ_{33}) and all shear stresses (σ_{12}, σ_{23} and σ_{31}). As a result, the constitutive equation for stress and strain used in the FE simulation was often based on true axial stress–strain curve, determined directly from the simple tensile test. Later, however, it was found that the ignorance of transverse normal stresses has caused inconsistency between simulation and experimental behaviour [1, 7, 14–16]. Consequently, various schemes were proposed to determine the correct constitutive equation for the FE simulation [4, 5]. The scheme used in the current study was slightly modified from that given in Ref. [5].

The constitutive equation for the FE simulation is based on Eq. 1. In the original scheme presented in Ref. [5], values for the parameters in Eq. 1 were selected in such a way that the corresponding stress–strain input curve fits the experimentally determined uni-axial stress–strain curve

and satisfies continuity of the first derivative at ε_y, ε_n and ε_t. FE model with this constitutive equation is used to generate the uni-axial engineering stress-elongation curve, which is compared with the experimental counterpart. Through iteration, discrepancy between the two curves is minimised by adjusting values for parameters in Eq. 1. The modified approach used in the current study is based on the same principle, but applies the iteration to each section of the stress–strain curve. That is, Young's modulus E in Eq. 1(a) is adjusted first to have the linear section of the FE-generated engineering stress-elongation curve be identical to that determined from the experiment. The process is then applied to Eq. 1(b) for the strain range from ε_y to ε_n, and then to Eq. 1(c) for the strain range from ε_n to ε_t. However, it was found that no matter what values were selected for parameters in Eq. 1(c), the engineering stress-elongation curve generated from the FE model could not match the experimental curve without sacrificing the accuracy of the cross-section reduction predicted from the FE model (the second criterion described earlier). In other words, if the FE-generated engineering stress-elongation curve were matched to the experimental curve, the cross-section in the FE model would be reduced much more than that measured experimentally. This was later found to be due to the ignorance of time-dependent deformation that must have occurred during the testing. Since glass transition temperature of HDPE is below −50 °C, time-dependent deformation is unavoidable at room temperature. However, with the neck evolvement, thus improvement of molecular chain alignment in the loading direction [29], the time-dependent deformation will eventually become negligible. As a result, the creep model was considered in the FE simulation, to reconcile the difference with the experimental measurement. But, the creep model was considered only during the initial necking process, not after the neck initiation was completed.

Creep model introduced in the FE simulation is based on the following strain rate function, expressed in terms of the power-law expression of stress and time [28]:

$$\dot{\tilde{\varepsilon}}^{cr} = A\tilde{q}^n t^m \tag{3}$$

where $\dot{\tilde{\varepsilon}}^{cr}$is the uni-axial-equivalent creep strain rate, $\tilde{q}$ the von-Mises equivalent stress, t time measured from the onset of necking, and A, n and m are the user-defined constants for which values were selected through a trial-and-error process. As to be shown in the "Results and discussion" section, the above function is sufficient to adjust the engineering stress-elongation curve from the FE model so that it could match the experimental curve using only one set of A, n and m values for each type of HDPE.

Note that the creep model was introduced only during the neck initiation, i.e. during the initial stress-drop section in the engineering stress-elongation curve, but not during the neck propagation. This is because molecular chains in a fully developed neck should be well aligned in the loading direction [29]. Therefore, their time-dependent deformation behaviour should become negligible. Although time-dependent deformation could still occur at the neck propagation stage, in sections of the specimen other than that for the neck initiation, such deformation only causes increase of elongation in the flow-stress section of the engineering stress-elongation curve, not affecting the level of flow stress that is used as a criterion to validate the FE model. Therefore, ignorance of creep deformation at the neck propagation stage should not affect accuracy of the constitutive equation. Creep deformation was not introduced before the maximum stress mainly to save computational time, as creep deformation should not be significant at that stage.

It should also be noted that for the two HDPEs used in this study, work hardening at the strain range for Eq. 1(d) was so significant that one set of parameter values for the equation was insufficient to introduce the required stress increase with the increase of deformation to match the experimental data. Instead, a minimum of four sets of values are needed for Eq. 1(d), with β kept constant at 1.8 (as recommended in Ref. [5]) but different k and M values. As to be shown later, the use of four sets of parameters for Eq. 1(d) provides sufficient strain hardening in the constitutive equation, in order to reproduce the flow stress and the cross-sectional reduction obtained from the experimental testing. The main advantage of the current approach over that used previously [4, 5] is that the former provides mathematical expression for the constitutive relationship between stress and strain in order to facilitate future analysis of deformation when subjected to multi-axial loading; while the latter only discrete data points.

Results and discussion

Experimental

Typical plots of engineering stress versus elongation for different specimen thicknesses are presented in Fig. 3a and b for PE1 and PE2, respectively. In general, variation of specimen thickness does not affect the curves up to the maximum point, with PE1 giving higher values of maximum engineering stress than PE2. After the maximum point, the curves show dependence on the specimen thickness, as characterised by the onset of neck propagation (point F in Fig. 4), flow stress level, and elongation at break. The general trend is that with decrease in specimen thickness, elongation at point F decreases, but flow stress and elongation at break increase as shown in Table 2.

Neck evolvement during the test is characterised by the change of width (W) and thickness (t) during the test, after

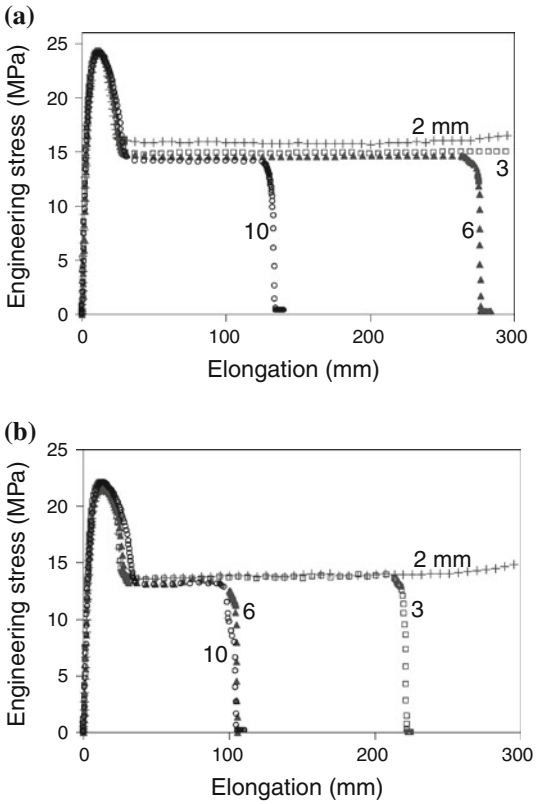

Fig. 3 Engineering stress-elongation plots determined from experiments at crosshead speed of 100 mm/min, for PE1 (**a**) and PE2 (**b**) of various specimen thicknesses: 2 mm (*plus*), 3 mm (*square*), 6 mm (*triangle*) and 10 mm (*circle*)

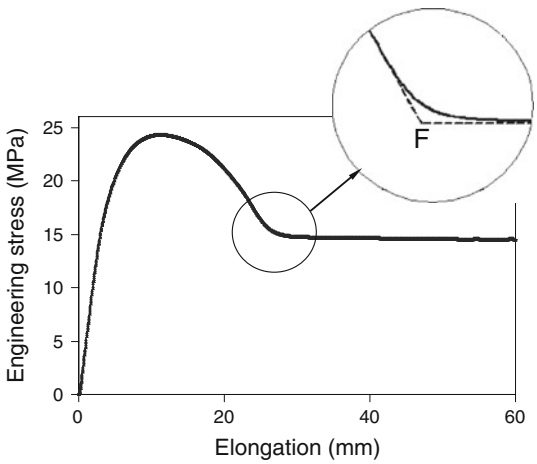

Fig. 4 Location of the critical point (point *F*) for onset of neck growth on a typical engineering stress-elongation plot

normalisation with their original dimensions (W_o and t_o, respectively). The ratio of normalised width to normalised thickness (named χ here) is plotted as a function of elongation in Fig. 5a and b, for PE1 and PE2, respectively. Those plots clearly indicate that with the decrease of specimen thickness, the difference between width contraction and thickness contraction is enlarged during the necking.

Percentage of the width reduction and the thickness reduction at point *F* (Fig. 4), $(1 - W_f/W_o)$ and $(1 - t_f/t_o)$, respectively, and the corresponding reduction in cross-sectional area $(1 - A_f/A_o)$ are presented in Fig. 6 as functions of specimen thickness. It is worth pointing out that variations of width and thickness with the change of initial specimen thickness are in an opposite trend, but the two trends converge at specimen thickness of around 13 mm. This is consistent with the expectation, as the aspect ratio for specimens of 13 mm thick should be around 1, thus showing no distinction in contraction between the two directions. Figure 6 also suggests that the reduction of cross-sectional area $(1 - A_f/A_o)$ increases with decrease of specimen thickness, though the change is relatively small compared to that for the width and thickness. Note that similar trend of dimensional contraction was also reported for PC/ABS blends [10], which was also attributed to the change of aspect ratio of the cross-section, but without any further explanation for the phenomenon.

In addition to the experimental data, Fig. 5 contains curves that were generated using the following equation to express χ as a function of elongation. The equation was adopted from the expression that is commonly used for the gain of Butterworth filter [30, 31], and with slight modification the experimental data can be fit by choosing suitable values for the constants. The expression captures the pattern of our data very well, though the data have nothing to do with the filtering function.

$$\chi = \frac{W/W_o}{t/t_o} = \left[\chi_f - \left\{ \frac{1}{\sqrt{\left[\left\{ 1 - 10^{\left(\frac{T-S}{K}\right)} \right\}^2 + \xi \times 10^{\left(\frac{T-S}{K}\right)} \right]}} \right\} \times (\chi_f - 1) \right] \quad (4)$$

in which K, ξ and S are adjusting factors, mainly for slope, curvature and horizontal shift, respectively, T is the elongation after normalisation with the crosshead speed (i.e. $T = \frac{\text{Elongation}}{\text{Crosshead speed}} \times 60$, where crosshead speed is 100 mm/min), and χ_f is χ value at point *F* shown in Fig. 4. Table 3 summarises values for K, ξ and S selected in this study for the curves to fit the experimental data. The values indicate that for a given HDPE, ξ and S can be kept constant. Only K needs to be changed with specimen thickness to fit the experimental data.

Using χ from Eq. 4 to take into account the difference in contraction between the width and the thickness directions,

Table 2 Mean values (and standard deviation) of critical parameters, each based on six measurements

Material	PE1				PE2			
Nominal thickness (mm)	10	6	3	2	10	6	3	2
Maximum engineering stress (MPa)	24.1 (0.1)	24.3 (0.1)	24.3 (0.2)	24.5 (0.4)	22.4 (0.3)	22.2 (0.3)	22.3 (0.2)	22.1 (0.4)
Elongation for F (mm)	30.1 (0.4)	27.2 (0.8)	23.8 (1.8)	22.8 (1.2)	31.7 (2.4)	28.6 (1.7)	25.0 (1.4)	25.9 (0.4)
Flow stress (MPa)	14.0 (0.1)	14.4 (0.1)	15.0 (0.1)	15.8 (0.1)	13.2 (0.1)	13.2 (0.1)	13.7 (0.1)	14.0 (0.2)
Elongation at break (mm)	146 (12)	202 (45)	440 (27)	More than 500	89 (7)	106 (3)	169 (43)	More than 500

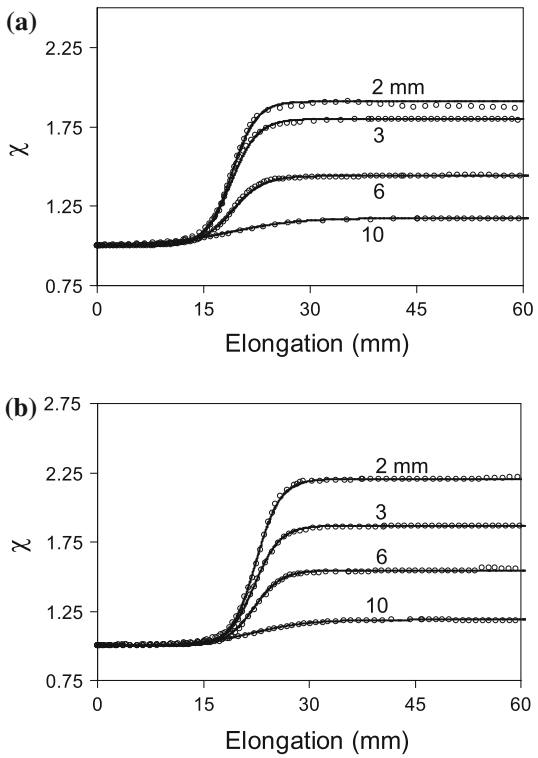

Fig. 5 Plots of χ, defined as the ratio of normalised width (W/W_o) to normalised thickness (t/t_o), as a function of elongation from experimental data (*circle*) and fitted data (*solid line*) using Eq. 4, for PE1 (**a**) and PE2 (**b**)

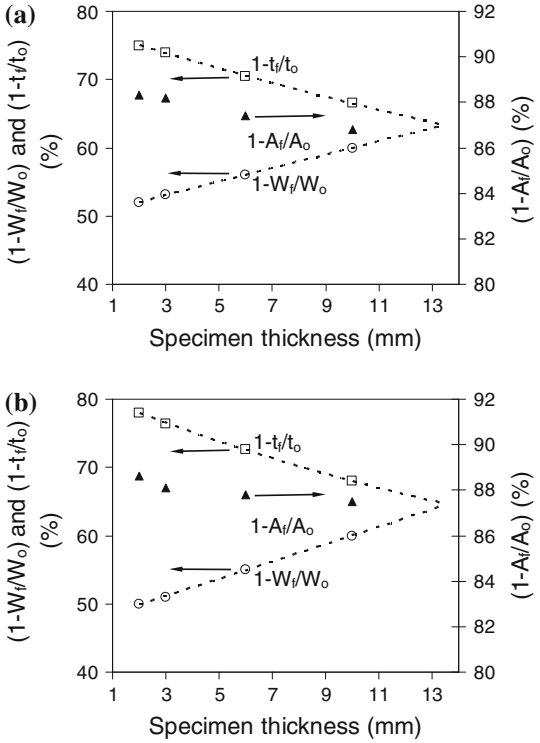

Fig. 6 Experimental data for variation of reduction in normalised width ($1 - W_f/W_o$) (*circle*), normalised thickness ($1 - t_f/t_o$) (*square*) and normalised area ($1 - A_f/A_o$) (*triangle*) as functions of specimen thickness, at the end of the neck formation but before its propagating to the neighbouring region, for PE1 (**a**) and PE2 (**b**)

axial true stress and strain values could be determined from the following equations, based on the measured load (P) and specimen width (W), with the assumption that volume is conserved during the plastic deformation.

$$\sigma_{\text{true}} = P\frac{W_o}{t_o}\frac{\chi}{W^2} \tag{5a}$$

$$\varepsilon_{\text{true}} = 2\ln\left[\frac{W_o}{W}\right] + \ln[\chi] \tag{5b}$$

Figure 7 presents typical true axial stress–strain curves from the two HDPEs of different thickness. The figure suggests that the change in specimen thickness has little effect on the stress–strain curve. Since thinner specimens show higher flow stress and more cross-section contraction, values for the maximum axial stress and strain at the point for the onset of neck growth are expected to be the largest for the thinnest specimens.

Table 3 Values for parameters in Eq. 4

Material	PE1				PE2			
Nominal thickness (mm)	2	3	6	10	2	3	6	10
K	2.4	2.6	3	6.5	2.4	2.55	2.7	5.5
ξ	4	4	4	4	4	4	4	4
S	12	12	12	12	14	14	14	14
χ_f	1.91	1.80	1.44	1.17	2.20	1.87	1.54	1.19

Figure 8 expresses the rate of neck length increase (Ω) as a function of specimen thickness for both PE1 and PE2.

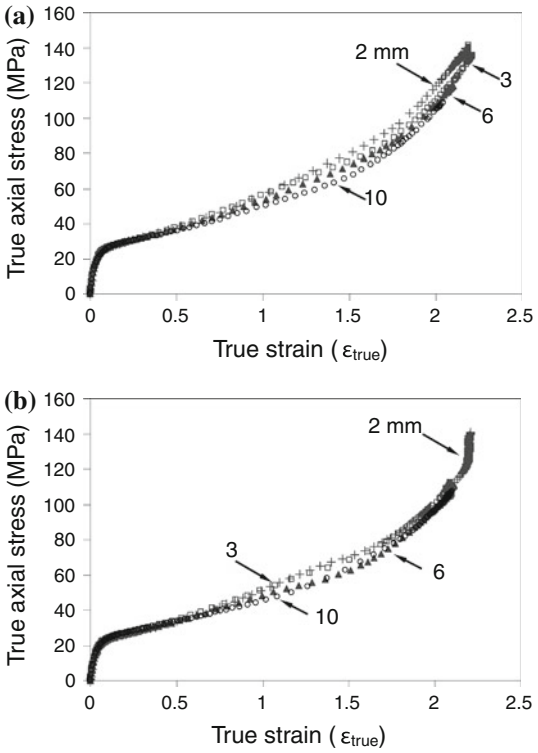

Fig. 7 Experimental curves of true axial stress versus true strain for PE1 (**a**) and PE2 (**b**): 2 mm (*plus*), 3 mm (*square*), 6 mm (*triangle*) and 10 mm (*circle*). Crosshead speed was 100 mm/min

The figure suggests that the neck growth rate (represented by Ω value) decreases with the decrease of specimen thickness for both HDPEs, with Ω value for PE2 being slightly higher than PE1. Since flow stress increases with decrease of specimen thickness, with the opposite trend for Ω, results from the experimental measurement suggest that the thinner specimens provide higher resistance to the neck growth.

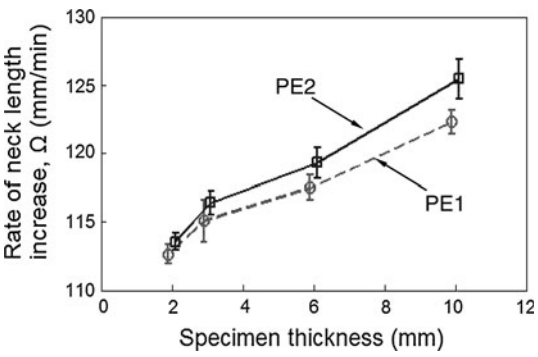

Fig. 8 Plot of the measured rate of neck length increase (Ω) as a function of specimen thickness for PE1 and PE2 at crosshead speed of 100 mm/min

Numerical simulation

Following the simulation procedure described in section II, values for parameters in Eqs. 1 and 3 are listed in Tables 4 and 5, respectively. An example of the neck formation in the FE model is given in Fig. 9 which was generated at elongation of 80 mm, using parameter values for 10-mm-thick PE1.

As mentioned earlier, the FE model for purely elastic–plastic deformation cannot generate both engineering stress-elongation curve and cross-sectional reduction that match those obtained experimentally. This was confirmed after numerous trials using different sets of values for parameters in Eq. 1. Examples of the engineering stress-elongation curve generated by the FE model for purely elastic–plastic deformation are presented in Fig. 10 (+), and compared with the experimental curve (solid line) from a 10-mm-thick PE1 specimen and another FE-generated

Table 4 Values of parameters for Eq. 1

Equation	Parameters	Materials			
		PE1		PE2	
		Specimen thickness (mm)		Specimen thickness (mm)	
		10	3	10	3
1(a)	ε_n	0.078	0.078	0.080	0.074
	E (MPa)	800	800	800	800
	v	0.35	0.35	0.35	0.35
1(b)	ε_y	0.013	0.013	0.008	0.008
	a	30	30	25	25
	b	0.015	0.015	0.025	0.025
	c	0.007	0.007	0.038	0.040
	d	−19	−19	−22	−23
	e	14	14	11	11
1(c)	ε_t	0.41	0.39	0.43	0.43
	αk	37	37	35	35
	N	0.14	0.14	0.16	0.16
1(d)					
1st part	k	30	30	28	28
	M	0.4	0.4	0.4	0.4
	β	1.8	1.8	1.8	1.8
2nd part	k	25	27	24	24
	M	0.5	0.5	0.5	0.5
	β	1.8	1.8	1.8	1.8
3rd part	k	16	22	19	19
	M	0.7	0.6	0.6	0.60
	β	1.8	1.8	1.8	1.8
4th part	k	5.9	19	10	10
	M	1.1	0.6	0.8	0.8
	β	1.8	1.8	1.8	1.8

Table 5 Values for parameters in Eq. 3

Materials	Nominal thickness (mm)	*A*	*n*	*m*
PE1	10	1.75E−08	4.5	−0.5
	3	1.75E−08	4.5	−0.5
PE2	10	2.50E−08	4.5	−0.5
	3	2.50E−08	4.5	−0.5

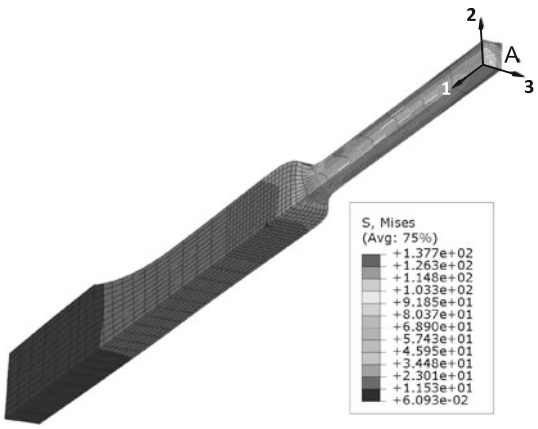

Fig. 9 FE model for PE1 of 10 mm thick at elongation of 80 mm

curve (□) with the consideration of creep deformation. Both FE-generated curves in Fig. 10 are from FE models that can mimic correctly the cross-sectional reduction observed experimentally. However, the one without creep does not match the experimental curve in the stress-drop section after the maximum point. Only with the creep deformation can the stress drop section be identical to that from the experiment.

Figure 11 compares the engineering stress-elongation curves for both HDPEs in two different thicknesses, 10 and 3 mm. With the consideration of creep, the FE-generated curve reproduces the experimental curve correctly,

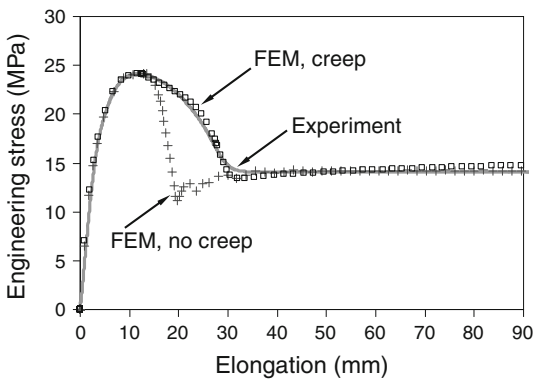

Fig. 10 Comparison of engineering stress-elongation curve between experiment (*solid line*) and FE simulation for PE1 of 10 mm thick. The latter is either with (*square*) or without (*plus*) the consideration of creep

matching the stress drop section, elongation for on-set of neck propagation (point *F* in Fig. 4), and flow stress level. Results from the FE model can also distinguish the small difference between two HDPEs in the stress level for the onset of neck propagation, 14 and 13 MPa for PE1 and PE2 of 10 mm thick, respectively, which are consistent with the values listed in Table 2.

Accuracy of the FE model for mimicking the deformation behaviour was evaluated by comparing the reduction of cross-sectional area during the necking process, for both 10- and 3-mm-thick specimens. As shown in Fig. 12 in which the cross-sectional area is normalised by its original value before the deformation, reasonable agreement is achieved for all comparisons.

Figure 13 presents a comparison of curves for true axial stress (σ_{11}) versus true strain between experiment and FE simulation, for 10- and 3-mm-thick specimens of both HDPEs. The experimental values (solid line) were calculated from load and cross-sectional area at the cross-section where neck was initiated, and the simulation counterparts (□) were determined in the same manner but from the FE model. The figure also includes curves of von Mises stress (triangle), which are used as the material property input for the FE simulation and presented here as reference for comparison. Note that the two σ_{11} curves in Fig. 13 are very close to each other, which further supports the representation of FE simulation for the deformation of HDPEs. Closeness of von Mises stress to σ_{11} in Fig. 13 suggests that σ_{11} dominates the von Mises stress value during the necking process. Based on the above comparisons, it is concluded that stress state determined from the FE model can be used to analyse the effect of aspect ratio (by changing specimen thickness) on the stress state generated during the necking process.

Figure 14 presents variation of nodal values for transverse normal stresses (σ_{22} and σ_{33}) at the central point (point *A* in Fig. 2) as a function of true strain (ε_{true}). Since shear stresses are very small and their variation during necking insignificant, their data are omitted in those plots for clarity. Figure 14 demonstrates the significance of variation in the transverse normal stresses during the necking process. Further, it highlights the opposite trend of the change of transverse normal stresses with the change of specimen thickness, i.e. σ_{22} (in the width direction) increases with the decrease of specimen thickness but σ_{33} (in the thickness direction) decreases. It should be pointed out that the maximum difference between the two transverse normal stresses occurs when the cross-section is close to its final dimensions, i.e. before the onset of neck propagation to the neighbouring regions.

The opposite trend of the two transverse normal stresses with the change of specimen thickness, as shown in Fig. 14, provides explanations for the opposite trend of

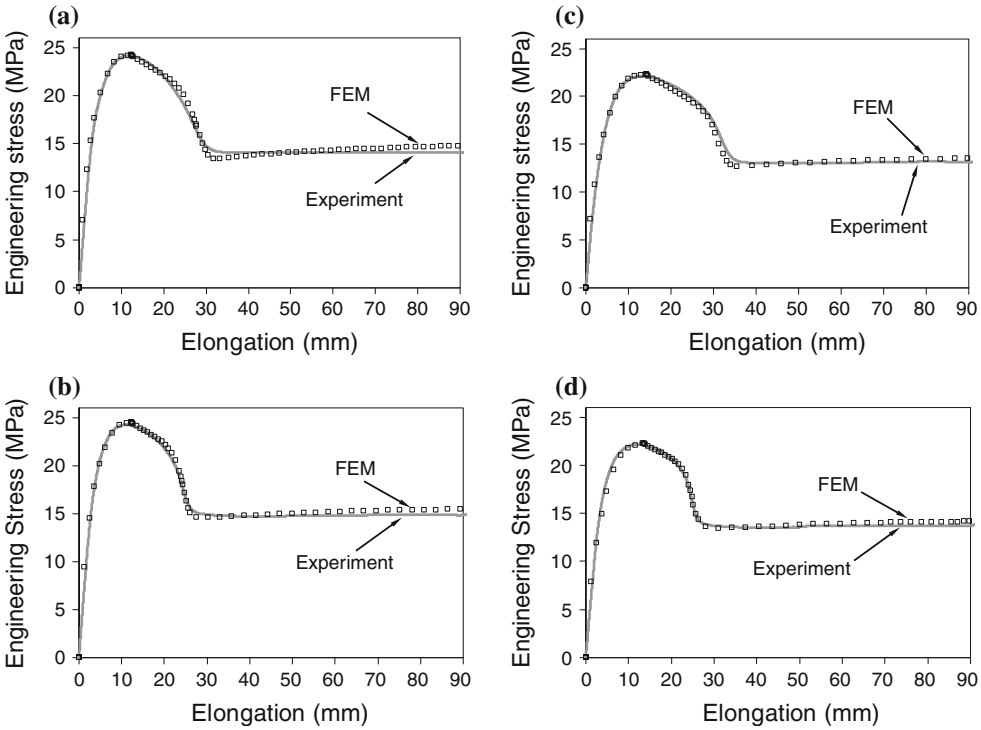

Fig. 11 Comparison of engineering stress-elongation curve between experiment (*solid line*) and simulation (*square*), for PE1 of 10 mm thick (**a**), PE1 of 3 mm (**b**), PE2 of 10 mm (**c**) and PE2 of 3 mm (**d**)

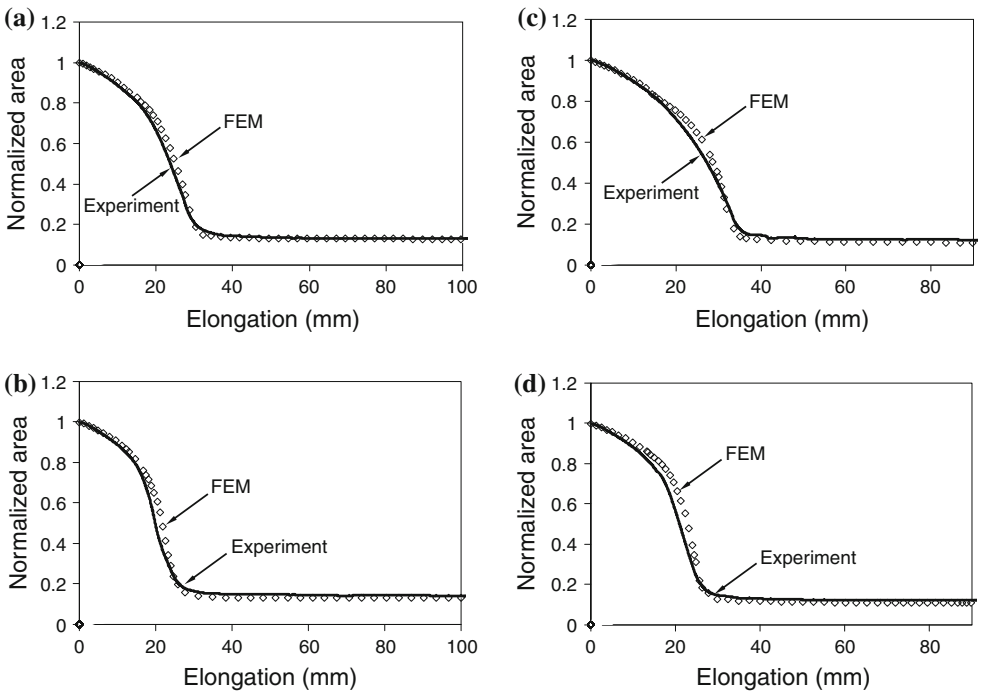

Fig. 12 Comparison of the change of normalised cross-sectional area at the initial necking section as a function of elongation between experiment (*solid line*) and FE simulation (*diamond*), for PE1 of 10 mm thick (**a**), PE1 of 3 mm (**b**), PE2 of 10 mm (**c**) and PE2 of 3 mm (**d**)

contraction in the width and thickness directions shown in Fig. 6. That is, with the decrease in specimen thickness used for the tensile testing σ_{22} increases due to the increase in the resistance to deformation, resulting in bigger W_f/W_o value (i.e. smaller contraction in the width direction); while the opposite trend applies to σ_{33} and contraction in the thickness direction. Figure 14 also suggests that as the specimen thickness approaches zero, σ_{33} ceases, thus plane stress condition prevails.

G'Sell et al. [9] suggested that during necking, variation of stress state can be divided into two stages. The first stage occurs at the beginning of the neck formation when the neck front approaches to the cross-section of interest. At this stage, the von Mises stress should be larger than the

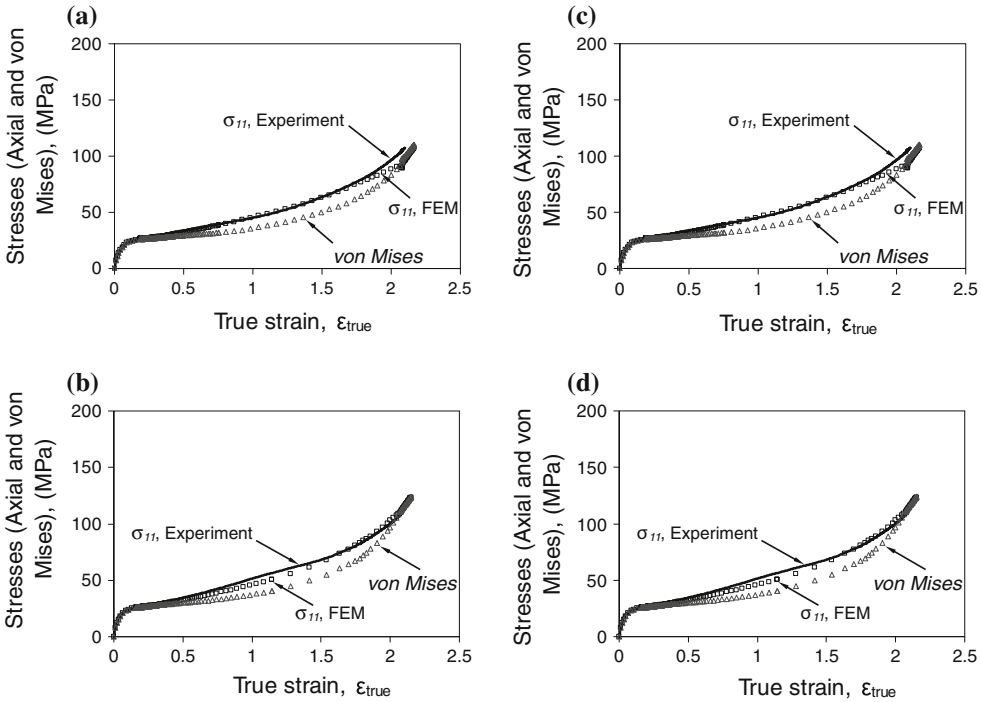

Fig. 13 Plots of true axial stress (σ_{11}) versus true strain (ε_{true}) in the initial necking section, determined from experiment (*solid line*) and FE simulation (*square*) for PE1 of 10 mm thick (**a**), PE1 of 3 mm (**b**), PE2 of 10 mm (**c**) and PE2 of 3 mm (**d**). Curve of von Mises stress (*triangle*) is also included as a reference. Note that the two curves for σ_{11} almost overlap with each other

axial stress due to the transverse stress being compressive. At the second stage when the cross-section is about to reach the final dimensions of the neck, however, the transverse normal stresses are tensile, thus the von Mises stress becomes smaller than the axial stress. This phenomenon is correctly predicted by the FE model, as shown in Fig. 15 for variation of the stress components at two cross-section locations, of 3.05 mm (Fig. 15a) and 6.11 mm (Fig. 15b) away from the neck initiation location, for 10-mm-thick PE1 specimen. Figure 15a and b shows that the von Mises stress is larger than the axial stress at the beginning of necking where sharp stress drop occurs, but smaller at the later stage. It also shows that the transverse normal stress (σ_{22}) is compressive at the beginning of the necking process, but it becomes tensile later. Thus, the general trend presented in Fig. 15 supports that suggested by G'Sell et al. [9].

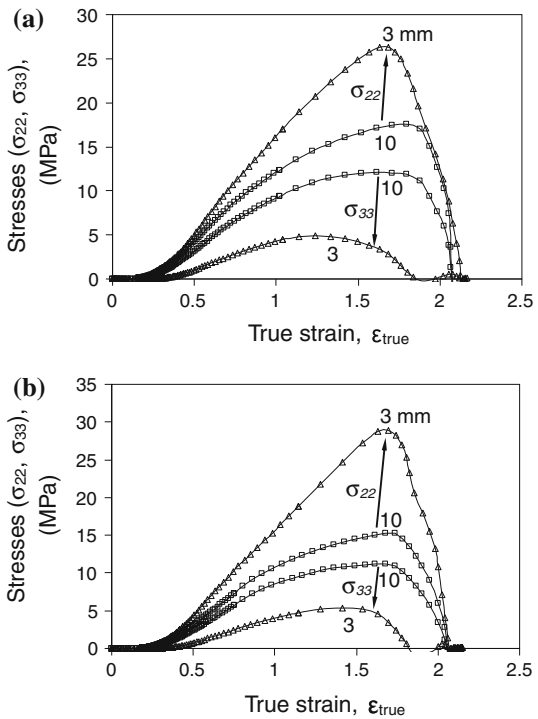

Fig. 14 Plots of transverse normal stresses (σ_{22} and σ_{33}) at point *A* in Fig. 2, as a function of true strain for PE1 (**a**) and PE2 (**b**), of 10 mm thick (*square*) and 3 mm thick (*triangle*). *Arrows* in the figures indicate the direction of change with the decrease of specimen thickness

It should be pointed out that the sharp drop of σ_{11} shown in Fig. 15a and b was generated before the neck front reached the point of interest, i.e. 3.05 and 6.11 mm away from the initial necking position for Fig. 15a and b, respectively. The sharp drop of σ_{11} was caused by force decrease due to the localised deformation at the initial necking position, but little change of the cross-sectional area (i.e. little strain change) at the point of interest. When the neck front reaches the point of interest, however, the cross-sectional area is reduced, thus causing increase in both σ_{11} and strain values. As suggested in Fig. 15, the onset of σ_{11} increases after its sharp drop occurs at strain levels about 0.43 and 0.32 for the locations of 3.05 and 6.11 mm, respectively, away from the initial necking position. In other words, further away is the point of interest from the initial necking position, lower is the strain level at which the necking process commences at that

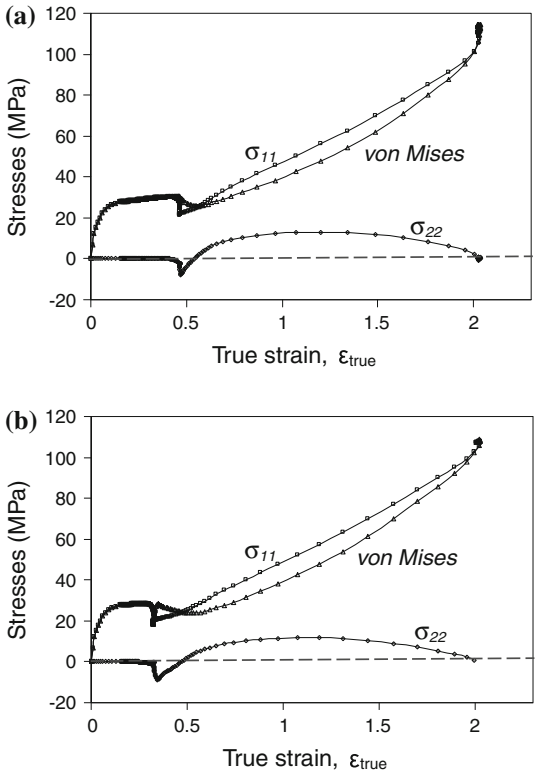

Fig. 15 Plot of normal stresses (σ_{11} and σ_{22}) and von Mises stress obtained from FE simulation as a function of true strain at a section of 3.05 mm (**a**) and 6.11 mm (**b**) away from the initial necking position (where point *A* is located in Fig. 2) for PE1 of 10 mm thick

point. This trend is consistent with the experimental observation in another study [5], and is attributed to the gradient of the cross-sectional reduction generated in the initial necking process.

Although results presented in this paper are expressed as a function of thickness variation, similar effects should also occur by varying the specimen width to change the aspect ratio. This is expected because the HDPE plates were compression-moulded, thus having isotropic mechanical properties.

Conclusions

The study provides information to quantify the influence of specimen thickness on the necking behaviour during uniaxial loading of HDPE. A three-dimensional finite element model was developed to facilitate determination of stress–strain relationship, and to provide explanations that elucidate the effect of aspect ratio of cross-section on the necking process.

Experimental results show slight dependence of engineering stress-elongation curve on the change of specimen thickness. The results show that necking in thinner specimens generates higher reduction in thickness direction but lower in width direction. The axial stress–strain curve, however, has little variation by the change of specimen thickness, except the stress and strain values at the completion of the neck initiation process. The data suggest that resistance to neck propagation is highest for the thinnest specimens, as their neck growth speed is lowest and flow stress highest.

The work also provides the constitutive relationship between stress and strain that can be used in the FE simulation to mimic the necking process. It was found that time-dependent deformation needs to be considered in order to regenerate accurately the experimental deformation behaviour. A simple, time-hardening form of power law function was found to be sufficient to describe the creep deformation observed in the study, and only one parameter in the power law function depended on HDPE properties used in the simulation. Engineering stress versus elongation, true axial stress versus strain, and normalised cross-sectional area versus elongation curves, from the FE simulation, all show close agreement with the experimental results.

The FE simulation suggests that with the decrease of specimen thickness, normal stress in the thickness direction decreases, while that in the width direction increases. This is consistent with the experimental observation that with decrease in specimen thickness, reduction of the specimen thickness increases by the necking process, but reduction in specimen width decreases. Decrease in specimen thickness used for testing also resulted in the increase in the maximum true strain generated by the necking process, which is consistent with the expectation that when the plane-stress condition dominates the deformation, capability of the material to endure deformation increases.

Acknowledgements The work was supported by Natural Sciences and Engineering Research Council of Canada (NSERC), NOVA Chemicals, and Queen Elizabeth II Ph.D. Graduate Scholarship at the University of Alberta. Sincere appreciation is also due to T. Hilvo for help in specimen preparation, B. Faulkner for fabrication of the extensometer used in the experiments, R. Adianto for assistance in machine operation for testing, and H. J. Kwon and S. Adeeb for invaluable advices in ABAQUS operation.

References

1. Neale KW, Tugcu P (1985) J Mech Phys Solids 33:323
2. Boyce MC, Arruda EM (1990) Polym Eng Sci 30:1288
3. Wu PD, Van Der Giessen E (1995) Int J Plast 11:211
4. Tomita Y, Hayashi K (1993) Int J Solid Struct 30:225
5. Kwon HJ, Jar P-YB (2008) Int J Solid Struct 45:3521
6. Li HX, Buckley CP (2008) Int J Solid Struct 46:1607
7. Fager LO, Bassani JL (1986) Int J Solid Struct 22:1243
8. Masud A (2005) Mech Adv Mater Struct 12:457
9. G'Sell C, Aly-Helal NA, Jonas JJ (1983) J Mater Sci 18:1731. doi:10.1007/BF00542069

10. Fang QZ, Wang TJ, Beom HG, Zhao HP (2009) Polymer 50:296
11. Buckley C, Costas M (2004) J Polym Sci Part B: Polym Phys 42:2081
12. G'Sell C, Jonas JJ (1979) J Mater Sci 14:583. doi:10.1007/BF00772717
13. Hutchinson JW, Neale KW (1983) J Mech Phys Solids 31:405
14. Tugcu P, Neale KW (1987) Int J Mech Sci 29:793
15. Tugcu P, Neale KW (1987) Int J Solid Struct 23:1063
16. Neale KW, Tugcu P (1988) Int J Numer Methods Eng 25:99
17. Peterlin A (1971) J Mater Sci 6:490. doi:10.1007/BF00550305
18. Kwon HJ, Jar P-YB (2007) Polym Eng Sci 47:1327
19. G'Sell C, Hiver JM, Dahoun A (2002) Int J Solid Structres 39:3857
20. Hill R (1952) J Mech Phys Solids 1:19
21. Bridgman PW (1944) Trans Am Soc Met 32:553
22. Ogden RW (1972) Proc R Soc London, Ser A 328:567
23. Hollomon JH (1945) Trans Metall Soc Am Inst Mining Metall Engrs 162:268
24. Spitzig WA, Sober RJ, Richmond O (1975) Acta Metall 23:885
25. Raghava R, Caddell RM (1973) J Mater Sci 8:225. doi:10.1007/BF00550671
26. Spitzig WA, Richmond O (1979) Polym Eng Sci 19:1129
27. Silano AA, Bhateja SK, Pae KD (1974) Int J Polym Mater 3:117
28. ABAQUS, Inc. (2007) Rate-dependent plasticity: creep and swelling, section 18.2.4, ABAQUS analysis user's manual. ABAQUS manual version 6.7
29. Peterlin A (1987) Colloid Polym Sci 265:357
30. Bianchi G, Sorrentino R (2007) Electronic filter simulation and design. McGraw-Hill Companies, New York
31. Butterworth S (1930) Exp Wirel Wirel Eng 7:536